Available online at www.sciencedirect.com
ScienceDirect
Trans. Nonferrous Met. Soc. China 34(2024) 1288−1299
Transactions of Nonferrous Metals Society of China
www.tnmsc.cn

Factors affecting reduction efficiency in industrial retorts for Mg production by aluminothermic process

Da-xue FU[1,2], Yao-wu WANG[1,2], Yue-zhong DI[1,2], Jian-ping PENG[1,2], Nai-xiang FENG[1,2]

1. Key Laboratory for Ecological Utilization of Multimetallic Mineral (Ministry of Education), Northeastern University, Shenyang 110819, China;
2. School of Metallurgy, Northeastern University, Shenyang 110819, China

Received 1 November 2022; accepted 9 June 2023

Abstract: Industrial experiments were carried out for Mg production by aluminothermic process in industrial retorts and the factors affecting the reduction efficiency were analyzed. The results show that the main factors reducing the reduction ratio are oxidation and combustion of crystallized magnesium and uneven mixing of raw materials. The latter could result in raw material regions with low Al concentration and MgO redundance, which can promote the formation of $12CaO·7Al_2O_3$ and $CaO·Al_2O_3$. For raw material regions with higher Al concentration, both MgO and CaO can be reduced to form the Mg_2Ca phase. Radiation and chemical reaction heat are the key factors affecting the reaction rate. Increasing the heating temperature can rapidly increase the bed temperature and obtain sufficient reaction ratio. The higher the magnesium content in the pellets is, the longer the reduction time is required.
Key words: magnesium metallurgy; vacuum aluminothermic reduction; Pidgeon process; heat transfer

1 Introduction

Lightweight magnesium-based materials have attracted worldwide attention because of their high specific strength and specific stiffness, good vibration reduction, magnetic shielding, corrosion resistance, and excellent workability and recovery. They are expected to have extensive applications in the manufacturing of automobile, aerospace, and medical equipment [1−3]. Over 80% of the global Mg production has been produced in China since 2010 [4], where the Pidgeon process is mainly used.

The Pidgeon process requires high energy input and discharges a large amount of CO_2 gases and residues [5], despite significant process development that reduced the energy consumption and CO_2 emission, such as automatic control [6−8] and regenerative combustion [9,10]. The high energy requirements result from the following two aspects: (1) a high reaction temperature (1473−1523 K) according to the thermodynamic theories [11] and (2) a long reduction time (8−12 h or longer) due to a slow chemical reaction rate as a result of a low mass transfer rate between solid−solid raw materials (dolime and ferrosilicon) compared with solid−liquid or solid−gas reactions [12]. The two factors not only increase the energy consumption, but also reduce the service life of industrial retorts (typically about 60 d) [13].

In contrast, aluminothermic processes have a lower reaction temperature and a faster reaction rate than the Pidgeon process [14,15], and have been proved to be feasible for Mg production under either vacuum [16,17] or normal atmosphere [18]. A lot of research has been carried out, including the effects of various factors on the reduction process [19,20], kinetics [16,21], and mechanism [22,23].

Corresponding author: Da-xue FU, E-mail: lllow@126.com
DOI: 10.1016/S1003-6326(24)66471-X

However, the high production cost of Al limits their industrial applications [11,14,24]. For the aluminothermic processes, the present research interests are value-added utilizations of the residue, for example, producing spinel refractories [17], aluminum hydroxide [25,26], or value-added product, such as magnesium intermediate alloys [27−29], in order to reduce the production cost. FENG and WANG [25] proposed a vacuum aluminothermic process by which magnesium is produced through aluminothermic reduction of a mixture of calcined dolomite and calcined magnesite. The reduction residue can be reused to produce $Al(OH)_3$. The reaction mechanism [22] and kinetics [30,31] of the aluminothermic process [25] were investigated in a bench scale, but required further validation from industrial-scale tests. For industrial processes, heat and mass transfer would be different when more pellets and larger retorts are used, thus affecting the reduction efficiency.

In this work, industrial experiments were carried out for Mg production by the aluminothermic process using a mixture of calcined dolomite and calcined magnesite as the raw materials. The factors affecting the reduction efficiency in the industrial process were analyzed and discussed. Finally, some suggestions on improvement of the aluminothermic process were given.

2 Experimental

The experiments were carried out in a factory in Liaoning Province, China. Figure 1 shows the experimental procedures and the main equipment.

(1) Calcinations of dolomite and magnesite

The raw materials used in this study were obtained from Dashiqiao in Liaoning Province, China. Table 1 gives the major compositions of magnesite and dolomite. The purity of aluminum scraps used as reduction agent is larger than 90 wt.%. The magnesite was calcined at 1173 K for 1.5 h, while the dolomite was calcined at 1473 K for the duration. Both magnesite and dolomite have particle sizes of 15−35 mm.

(2) Milling and briquetting

The calcined dolomite and magnesite were pulverized in a ball mill. Then, they were mixed with aluminum at a mass ratio of calcined dolomite to calcined magnesite to aluminum to be 1:2.1:1.1 since the reaction was expected as Eq. (1). The mixture was pressed into pellets by a twin roller machine.

$$CaO{\cdot}MgO+5MgO+4Al=6Mg+CaO{\cdot}2Al_2O_3 \quad (1)$$

(3) Reduction

About 130 kg pellets were charged into a retort, which was maintained a vacuum of ~10 Pa and

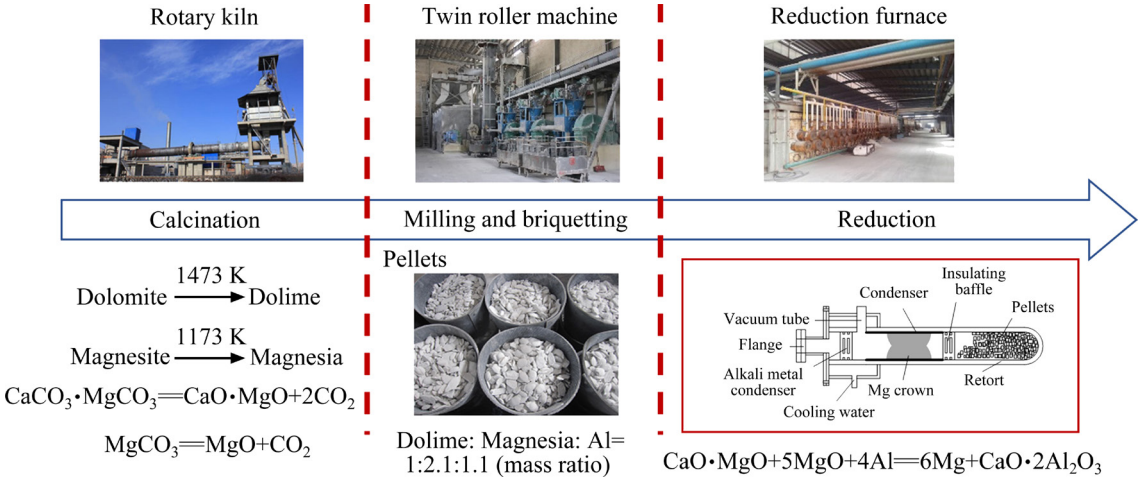

Fig. 1 Experimental procedures and main equipment

Table 1 Major chemical compositions of dolomite and magnesite (wt.%)

Ore	MgO	CaO	SiO_2	Fe_2O_3	Al_2O_3	Na_2O	Ignition loss
Dolomite	20.73	31.12	0.89	0.12	0.1	0.08	46.53
Magnesite	46.28	1.2	0.78	0.56	0.1	0.09	51.27

heated in a reduction furnace. The magnesium vapor released from the reaction zones of the retorts was condensed into crowns along the inner circumferences in the cooler zone of the retorts. The temperature in the retort cannot be measured in the industrial process and it is usually controlled by the temperature of the reduction furnace. It should be noted that the temperature of the reduction furnace is fluctuating and the temperature control has a certain lag. The experimental process controlled the temperature of the reduction furnace at 1483−1503 K or 1453−1473 K. In practice, the temperature difference between the retort and the reduction furnace is about 30−40 K. Therefore, the maximum temperature in the retort is about 1443−1473 K or 1413−1443 K. The experimental conditions are as follows: reduction time 8 h, reduction temperature 1443−1473 K (A); reduction time 10 h, reduction temperature 1443−1473 K (B); reduction time 10 h, reduction temperature 1413−1443 K (C).

The extraction extent of Mg is described as raw material-to-magnesium ratio (RMMR) or reduction ratio. The RMMR is defined as the ratio of the pellets mass before reduction to the crystallized magnesium mass, as shown in Eq. (2). The reduction ratio is defined as the ratio of the crystallized magnesium mass to the initial magnesium mass in the pellets, as shown in Eq. (3):

$$c=W_0/W_1 \quad (2)$$

$$\eta=[W_1/(aW_0)]\times100\% \quad (3)$$

where W_1 is the magnesium mass in the crystallizer, kg; W_0 is the total mass of pellets in the retort before reduction, kg; c is the RMMR; η is the reduction ratio, %; a is the content of Mg in the pellets and the value is 35.6% in this work.

3 Results and discussion

3.1 Results of industrial experiments

The reduction ratios and the RMMRs are given in Table 2. Temperature has a significant effect on the RMMR and the reduction ratio. The RMMRs of the aluminothermic process in the industrial experiments are lower, while the reduction ratios are lower than those of the Pidgeon process. The reduction ratio is also lower in the industrial process than in the bench scale.

3.2 Crystal morphology of Mg and reasons for decreasing reduction efficiency

Oxidation and combustion of crystallized magnesium is one of the reasons resulting in the low reduction ratio. In the industrial experiments, the crystallized magnesium was removed from the retort at the experimental temperature (1413−1473 K). The crystallized magnesium with a high temperature was easily oxidized and combusted, which reduced the Mg yield and thus lowered the reduction ratio. Figure 2 shows the morphology of the crystallized magnesium obtained from the industrial process. Crystallized magnesium with a compact columnar structure was obtained in the aluminothermic process (Figs. 2(a, b)). On the upper surface of the columnar crystals, there were compact crystallized magnesium particles with different sizes (Fig. 2(c)). Some of the crystallized magnesium showed melting signs (Fig. 2(d)) and the particles had rounded edges (Fig. 2(e)). The EDS analysis in Fig. 2(f) shows that the particle surface was oxidized. In contrast, the oxidation level was low inside the columnar crystals (Fig. 2(a)). Dendritic crystallized magnesium was obtained in the Pidgeon process (Fig. 2(g)). The particles edges were clear, the gaps between branches were large, and there were no melting signs (Fig. 2(h)). The surface of the dendritic crystallized magnesium was also oxidized as suggested by EDS analysis in Fig. 2(i). According to thermodynamic calculation, at 1473 K, the equilibrium partial pressure of magnesium vapor in

Table 2 Results of RMMR (c) and reduction ratio (η) in experiments

Process	Experiment	Experimental condition	c	η/%	Source
Alumino-thermic process	Industrial A	1443−1473 K, 8 h	4.6:1	61	This work
	Industrial B	1443−1473 K, 10 h	5.2:1	54	
	Industrial C	1413−1443 K, 10 h	6.2:1	45	
Pidgeon process	Bench scale	1473 K, 1 h	−	85	Ref. [30]
	Industrial data	1473 K, 10 h	(6.2−6.5):1*	75−83	Ref. [32]

*Data source: Production practice

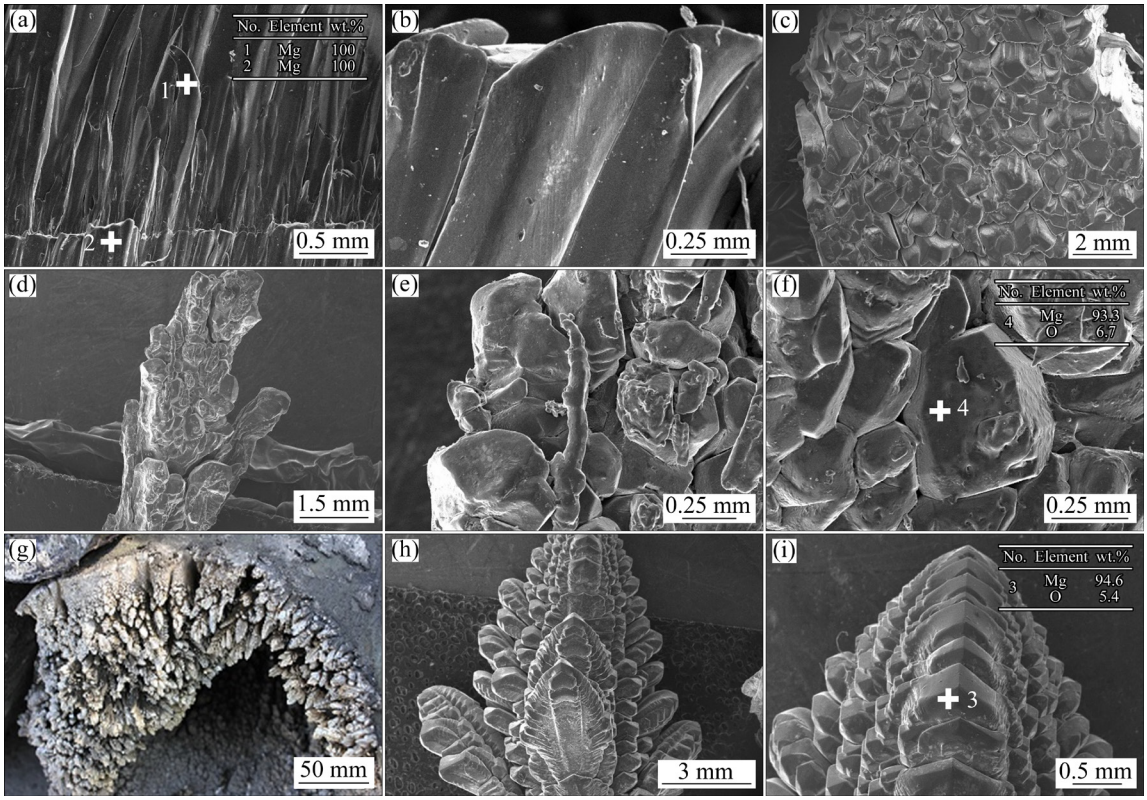

Fig. 2 Crystallized magnesium obtained in factory in this work (a−f) and by Pidgeon process (g−i)

the aluminothermic process (2.3×10^4 Pa) is about 7 times that in the Pidgeon process (3.2×10^3 Pa), which indicates that the aluminothermic process generates more magnesium vapor. Moreover, the reaction rate of the aluminothermic process is also higher than that of the Pidgeon process. Therefore, the condensation of Mg in the aluminothermic process releases more heat, resulting in the melting signs of the crystallized magnesium.

Flocculent magnesium produced in the later stage of the reduction resulted in the combustion of the crystallized magnesium. Figure 3 shows the crystallized magnesium morphology obtained in the lab. The crystallized magnesium had a compact structure and a small particle size in a range of dozens of microns to 100 μm (Fig. 3(a)). In Fig. 3(b), the particle edges were clear and angular, and there are no melting signs. Some floccules were found between the particles and were identified as Mg by EDS analysis. The flocculent magnesium mainly concentrated among particles. It is speculated that these flocculent magnesium metals were produced in the later stage of the reduction. The flocculent magnesium was only found in the lab tests since the crystallized magnesium was removed from the retort at room temperature. Compared with the results obtained in the lab, it is deduced that the flocculent magnesium was also produced in the industrial process. However, the flocculent magnesium metals easily oxidized and combusted in the industrial process since the crystallized magnesium was removed from the retort at high temperature. In some cases, the combustion of the flocculent magnesium could cause the combustion of other crystallized magnesium particles, which significantly increased RMMR and decreased the reduction ratio.

The crystallized magnesium adjacent to the crystallizer wall also easily oxidized and contained more impurities. Figure 3(c) shows the crystallized magnesium adjacent to the crystallizer wall, which had smaller particle sizes and was porous. The small particles are attributed to the low crystallization temperature and high phase transformation driving force. This leads to the formation of a large number of crystal nuclei and no enough time for the crystal growth. The crystallized magnesium contains the elements of O and Na according to the EDS analysis in Fig. 3(d). Therefore, it is important to improve the purity of

this part of magnesium to increase the yield of magnesium.

3.3 Effects of mixing of raw materials on phase transition

The uneven mixing of raw materials is another reason for the low reduction ratio. Figure 4 shows that Mg_2Ca alloy was produced during the industrial experiments. A special fungiform crystal was found in the crystallizer (Fig. 4(a)), which had metallic luster (Fig. 4(b)). It was relatively easier to fracture in comparison with the crystalline magnesium by hitting with a hammer. The fungiform crystal was Mg_2Ca by XRD analysis (Fig. 4(c)).

Figure 5 shows the XRD pattern of the corresponding reduction slag. The main phases are $12CaO·7Al_2O_3$, $CaO·Al_2O_3$ and unreacted MgO. It is speculated that the possible reactions are Eqs. (4) and (5), instead of Eq. (1) as designed. According to a previous study [22], if there is enough Al_2O_3 phase, the phase transformation of calcium aluminate follows the sequence of $12CaO·7Al_2O_3 \rightarrow CaO·Al_2O_3 \rightarrow CaO·2Al_2O_3$ and the final product should be $CaO·2Al_2O_3$ [15]. This indicates that the reductant Al is insufficient, which may result from the uneven mixing of the raw materials (Fig. 6). The particle sizes of the calcined dolomite and the calcined magnesite are in the range of 1−100 μm, while the particle sizes of the reductant Al are in millimeters to avoid combustion and explosion of fine aluminum powders. The fine particles of the calcined dolomite and the calcined magnesite tend to penetrate through the skeleton composed of

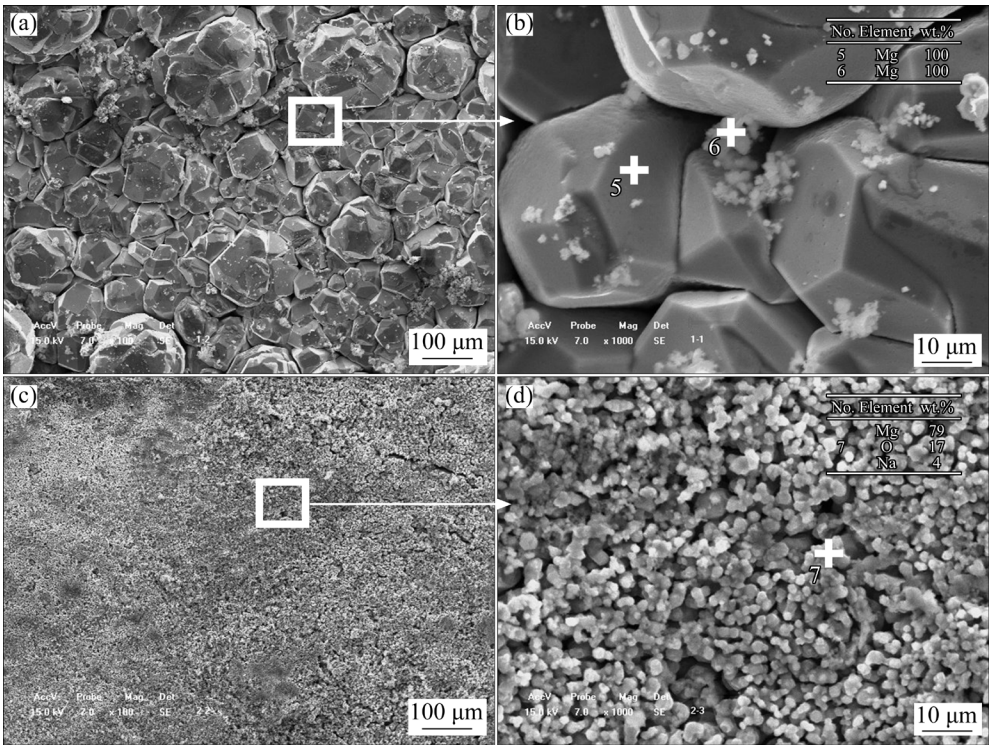

Fig. 3 Crystalline magnesium obtained in lab by aluminothermic process: (a, b) Top surface; (c, d) Back surface

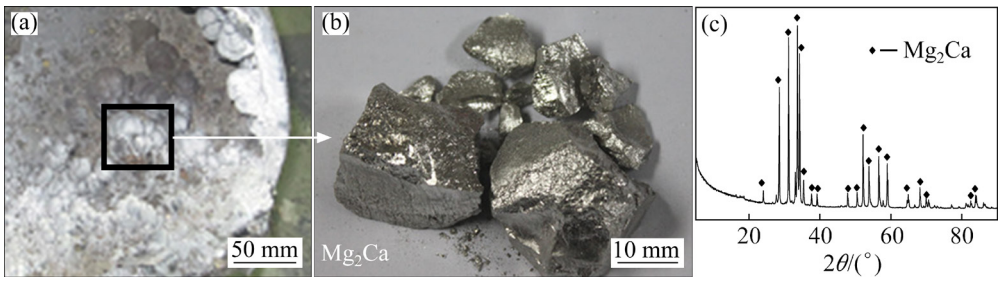

Fig. 4 Production of Mg_2Ca alloy during industrial experiments: (a) Fungiform crystal in crystallizer; (b) Fungiform crystal; (c) XRD pattern of fungiform crystal

aluminum scraps during the mixing process, resulting in the uneven mixing of the raw materials. For Al-poor raw materials, the reactions occurred according to Eqs. (4) and (5); for Al-rich raw materials, calcium vapor was produced by the reactions between Al and CaO in the calcined dolomite according to Eqs. (6) and (7). The Mg_2Ca alloy was formed from the condensation of the calcium vapor and magnesium vapor in the crystallizer.

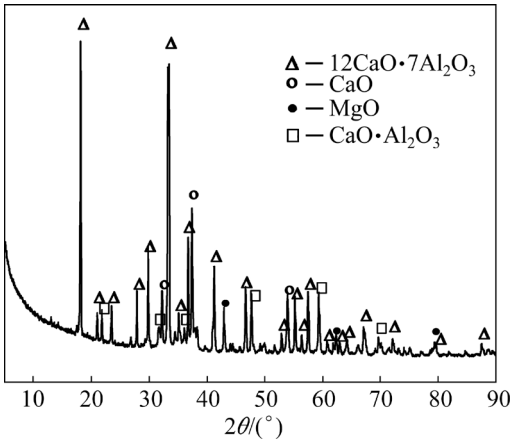

Fig. 5 XRD pattern of reduction residue of Al-poor raw materials

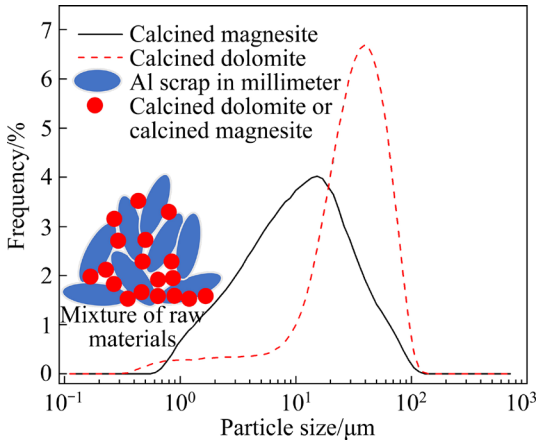

Fig. 6 Particle size distribution and schematics of uneven mixture of raw materials

$$12(CaO\cdot MgO)+9MgO+14Al=21Mg+12CaO\cdot 7Al_2O_3 \quad (4)$$

$$CaO\cdot MgO+2MgO+2Al=3Mg+CaO\cdot Al_2O_3 \quad (5)$$

$$33CaO+14Al=21Ca+12CaO\cdot 7Al_2O_3 \quad (6)$$

$$4CaO+2Al=3Ca+CaO\cdot Al_2O_3 \quad (7)$$

3.4 Numeric model of industrial retorts

Furthermore, the heat transfer in the industrial retorts is also one of the main factors affecting the reduction ratio. In Table 2, the reduction ratios in the industrial experiments were smaller than those in the bench scale. This phenomenon was also found in the Pidgeon process. Some studies have been carried out to explain the phenomenon in the Pidgeon process by numerical simulation [32−34]. These results showed that heat transfer in the industrial retort has a significant effect on the reduction ratio in the Pidgeon process. Similar numerical simulation was also done in this study to characterize the heat transfer in the aluminothermic process. The geometric model is shown in Fig. 7.

The retort closed at one end is inserted into the reduction furnace (Fig. 7(a)). It is heated in the furnace and the heat is transferred to the pellets through the retort wall (Fig. 7(b)). The retort has a

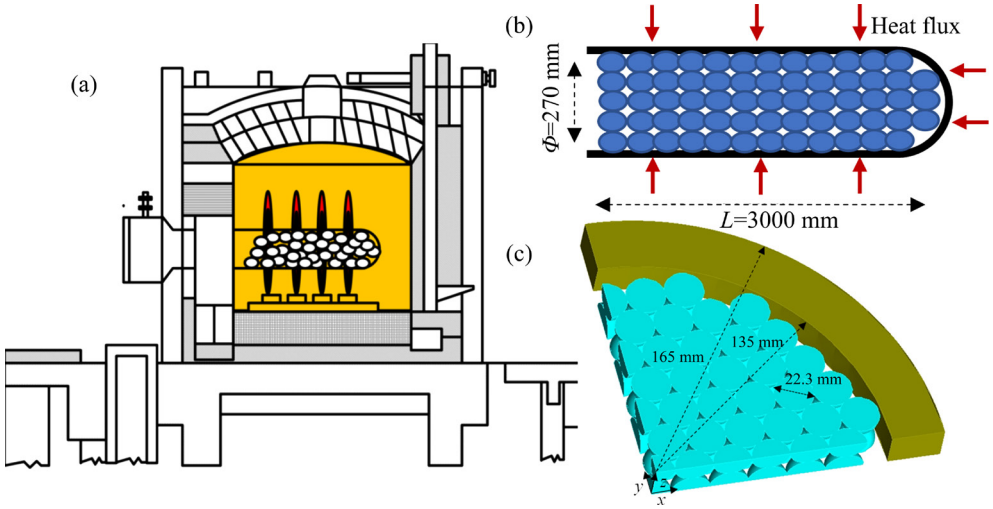

Fig. 7 Schematic diagram of furnace (a), reduction retort (b), and geometric model (c)

length of 2700−3000 mm and an inner diameter of 270 mm. The following assumptions were made: (1) The temperature gradient along length direction of the retort was ignored due to a large length-to-diameter ratio (about 10:1) of the retort. As a result, two half-pellet layers in longitudinal section was taken as the computational domain. (2) Walnut-shaped pellets were assumed to have equivalent volume to spherical ones and the average diameter of 22.3 mm [35] was used. The pellets charged in the retort was arranged in rhombic accumulation as shown in Fig. 7(c) since the porosity was close to the actual porosity. (3) The conduction heat transfer was neglected in the residue gas between the pellets since the process was carried out in vacuum.

The equations describing heat transfer in the retort in the Cartesian coordinate were expressed as Eqs. (8) and (9).

For the pellets:

$$\frac{\partial(\rho_{\mathrm{p}}C_{\mathrm{p}}T)}{\partial t}=(\frac{\partial^2}{\partial x^2}+\frac{\partial^2}{\partial y^2}+\frac{\partial^2}{\partial z^2})\cdot(\lambda_{\mathrm{p}}T)+(-M\Delta H\frac{\mathrm{d}\eta(t,T)}{\mathrm{d}t}) \tag{8}$$

For the retort:

$$\frac{\partial(\rho_{\mathrm{r}}C_{\mathrm{r}}T)}{\partial t}=(\frac{\partial^2}{\partial x^2}+\frac{\partial^2}{\partial y^2}+\frac{\partial^2}{\partial z^2})\cdot(\lambda_{\mathrm{r}}T) \tag{9}$$

where ρ is the density, C is the specific heat capacity, λ is the thermal conductivity, the subscript "p" represents pellet, the subscript "r" represents retort, T is the temperature, t is the time, M is the Mg maximum content per volume in the pellets, ΔH is the enthalpy for Reaction (1), η is the reduction ratio, and $\mathrm{d}\eta(t,T)/\mathrm{d}t$ is the reaction rate. Steel was chosen as the retort material. The values of the physical parameters are listed in Table 3. The reaction rate $\mathrm{d}\eta(t,T)/\mathrm{d}t$ in Eq. (8) is derived from the previous work [30].

The radiation between the pellets is calculated by S2S model, as shown in Eq. (10). The energy flux leaving a given surface $q_{\mathrm{out},k}$ is composed of directly emitted energy and reflected energy. The reflected energy flux is dependent on the incident energy flux from the surroundings, which then can be expressed in terms of the energy flux leaving all other surfaces. The amount of incident energy upon a surface from another surface is a direct function of the surface-to-surface "view factor," F_{kj}, which can be calculated by Eq. (11):

$$q_{\mathrm{out},k}=\varepsilon_k\sigma T_k^4+\rho_k\sum_{j=1}^{N}F_{kj}q_{\mathrm{out},j} \tag{10}$$

$$F_{kj}=\frac{1}{A_k}\int_{A_k}\int_{A_j}\frac{\cos\theta_k\cos\theta_j}{\pi r^2}\delta_{kj}\mathrm{d}A_k\mathrm{d}A_j \tag{11}$$

where $q_{\mathrm{out},k}$ is the energy flux leaving the surface k, ε_k is the emissivity, σ is the Stefan−Boltzmann constant, A_k is the area of surface and F_{kj} is the view factor between surface k. θ is the angle between a ray tracing and the normal vector at a point on the surface, r is the curvature radius at a point of the radiating surface, and δ_{ij} is determined by the visibility of $\mathrm{d}A_j$ to $\mathrm{d}A_k$. δ_{ij}=1 if $\mathrm{d}A_j$ is visible to $\mathrm{d}A_k$ and 0 otherwise.

Table 3 Physical parameters used in this work

Parameter	Value
Pellet density, ρ_{p}/(kg·m^{-3})	2100−748η
Specific heat capacity of pellet, C_{p}/(J·kg^{-1}·K^{-1})	1164.5+0.06T
Thermal conductivity of pellet, λ_{p}/(W·m^{-1}·K^{-1})	0.13+1.36×10^{-4}T (T<933 K); 0.05+2.14×10^{-4}T+(3.63×10^{-5}T−0.05)α (T≥933 K)
Enthalpy for Reaction (1), ΔH/(J·mol^{-1})	187182.5−11.6T
Mg maximum content in pellet, M/(mol·m^{-3})	30625
Retort density, ρ_{r}/(kg·m^{-3})	8030
Specific heat capacity of retort, C_{r}/(J·kg^{-1}·K^{-1})	502.5
Thermal conductivity of retort, λ_{r}/(W·m^{-1}·K^{-1})	16.3

The boundary and initial conditions are listed as follows:

Central axis of the retort: $\left.\frac{\partial T}{\partial z}\right|_{\substack{x=0\\y=0}}=0$

Outer wall of the retort: $T\left|_{x^2+y^2=R^2}\right.=T_{\mathrm{const}}$ (R is the outer radius of the retort)

Initial condition: T=298.15K

Tetrahedral mesh was used in the study. A series of mesh numbers 1.5×10^5, 3.0×10^5, and 4.5×10^5 were tested to take the mesh independence into account. The results of total reduction ratio at specific time durations are listed in Table 4.

The mesh number of 3.0×10^5 was chosen in the following calculation since a very small difference was observed between the mesh numbers of 3.0×10^5 and 4.5×10^5.

The reduction ratio in the numeric study (η_{cal}) is calculated according to Eq. (12):

$$\eta_{cal}=\frac{\sum_{pellet}(\eta_{cell}\cdot V_{cell})}{\sum_{pellet}V_{cell}} \tag{12}$$

where η_{cell} is the reduction ratio in a cell calculated by the experimental reaction rate; V_{cell} is the volume of the cell; $\sum_{pellet}V_{cell}$ represents the total volume of the charged pellets.

3.5 Heat transfer in industrial retorts

There is a large temperature gradient in the bed, resulting in an uneven reduction of the pellets. Figure 8 shows simulation results of the aluminothermic process. In Fig. 8(a), a large temperature gradient exists in the bed and the central temperature is the lowest due to heat transfer from the outside to the inside layer by layer. The result is consistent with Pidgeon process [34,36]. The temperature gradient leads to different reduction ratios of the pellets in the bed, as shown in Fig. 8(b). The reduction ratios of the pellets in the surrounding region are larger than those in the central region. By comparing the temperature profiles at 1448 and 1473 K in Fig. 8(a), it is deduced that the higher the heating temperature is, the higher the central temperature of the bed is. In other words, increasing the heating temperature improves the heat transfer driving force and helps rapidly increase the bed temperature. The pellets can thus obtain a high reaction rate and a high reduction ratio. The reduction ratio increases by about 5% for every 25 K increases after 8−10 h, as shown in Fig. 8(c). The calculated reduction ratio is 75.3% at 1448 K (close to the experimental temperature) for 8 h. The experimental reduction ratio is lower than the calculated value due to the combustion of crystallized magnesium and the uneven mixing of raw materials as mentioned above.

Table 4 Reduction ratio at different reduction time with different mesh numbers (1448 K) (%)

Mesh number	Reduction time/h									
	1	2	3	4	5	6	7	8	9	10
1.5×10^5	16.4	33.7	47.1	56.8	63.7	68.4	72.4	76.1	79.1	81.7
3.0×10^5	15.7	32.8	46.1	55.8	62.8	67.5	71.5	75.3	78.4	81.1
4.5×10^5	15.6	32.5	45.7	55.4	62.6	67.3	71.4	75.2	78.3	81.0

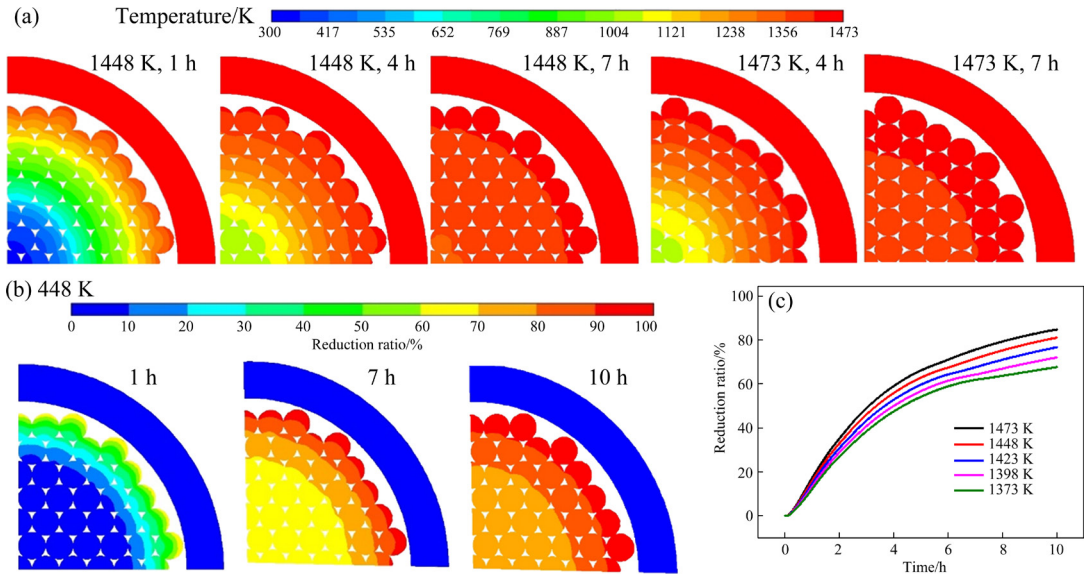

Fig. 8 Simulation results of aluminothermic process: (a) Temperature profiles at 1448 K and 1473 K; (b) Reduction ratio profiles at 1448 K; (c) Effects of temperatures on reduction ratio

In short, the temperature of the pellets in the bed is a limiting factor for the aluminothermic process. Increasing the heating temperature is helpful to rapidly increase the bed temperature, so that the pellets can obtain sufficient reaction rates, thus improving the overall reduction ratio and reducing the reduction time.

Radiation and chemical reaction heat are the key factors affecting the temperature in the bed, as be shown in Fig. 9. Heat transfer in the retort includes at least six ways (Fig. 9(a)): heat conduction within individual pellets, heat conduction between pellets through surfaces in contact, heat radiation among pellets, heat radiation between pores, heat conduction of molten alloys on the contact surface, heat conduction by solid−molten alloys−solid, and so on. In numerical computation, these kinds of heat transfer could be simplified to three main ones: radiation and heat conduction from the retort wall, heat conduction between briquettes, and radiation between briquettes and voids. In short, the heat conduction and radiation in the bed are considered in the calculation since there is no convective heat transfer in vacuum. Figures 9(b, c) show the effects of heat conduction, radiation, chemical reaction heat on the radial temperature distribution. When there is no radiation, it is difficult for the central temperature to reach the target one regardless of whether there are chemical reactions or not. When there is radiation, the central temperature increases with time until it approaches the target one. This indicates that the radiation is crucial to increasing the bed temperature. The chemical reaction decalescence reduces the temperature rise rate in the bed. The bed temperature with the reaction heat is lower than that without the reaction heat. The central temperature of the packed bed rapidly increases in the later stage of reduction since the reduction reactions are nearly complete and effects of the reaction heat on the temperature are weakened. The chemical reaction decalescence is proportional to the content of Mg in the pellets according to Eq. (8). Figure 9(d) shows the effect of Mg content in the pellets on the

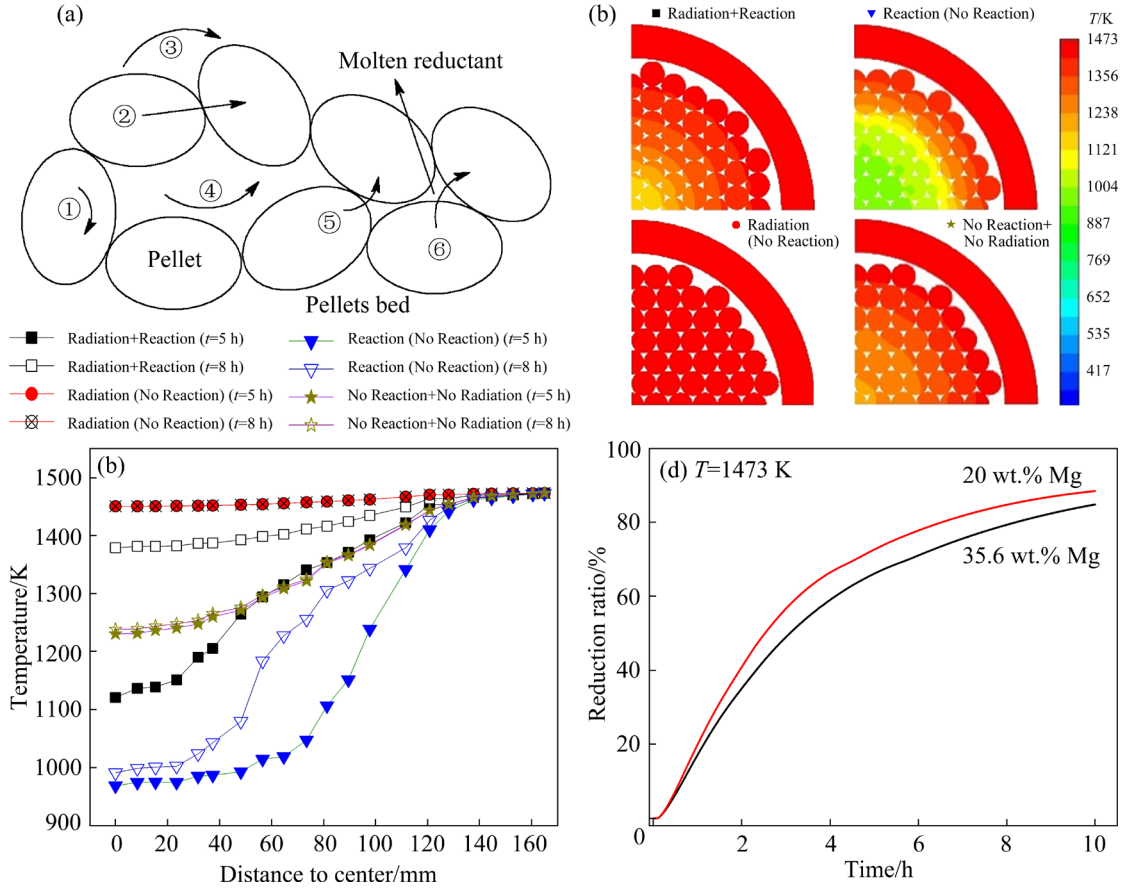

Fig. 9 Effects of chemical reaction heat and heat transfer on aluminothermic process: (a) Heat transfer in pellets bed; (b) Radial temperature distribution; (c) Temperature profiles at t=5 h; (d) Effects of Mg content in pellets on reduction ratio (t is reduction time; "Radiation" is radiative heat transfer; "Reaction" is chemical reaction heat))

reduction ratio with the assumption that the two cases have the same reaction rate. The reduction ratio increases when Mg content in the pellets reduces from 35.6% to 20% (a typical Mg content in the Pidgeon pellets). However, this would reduce magnesium yields. Therefore, it is deduced that the aluminothermic process, due to the higher Mg content in the pellets, would need longer reduction time than the Pidgeon process to obtain the same reduction ratio, although the reaction rate of the aluminothermic process is faster.

Although several factors were found to reduce the reduction efficiency in the industrial process, the aluminothermic process can still be an attractive alternative if the following improvements were to be achieved: (1) reducing the crystallized magnesium temperature to avoid combustion of crystallized magnesium; (2) using raw materials with similar particle sizes to improve mixing; (3) strengthening heat transfer in the retort to shorten the reduction period of the aluminothermic process.

4 Conclusions

(1) The surface of the crystallized magnesium was oxidated since the crystallized magnesium was removed from the retort at the reduction temperature (~1473 K). Flocculent magnesium was produced in the later stage of the aluminothermic reduction process, which easily combusted and then caused combustion of the crystallized magnesium.

(2) The Mg_2Ca alloy was produced due to the uneven mixing of raw materials. The phases of $12CaO·7Al_2O_3$ and $CaO·Al_2O_3$ were produced from the Al-poor raw materials and calcium vapor was produced from the Al-rich raw materials.

(3) The temperature of the pellets in the bed is a limiting factor for the aluminothermic process. Increasing the heating temperature is helpful to rapidly increase the bed temperature. The reduction ratios of the pellets in the bed are uneven due to the large temperature gradient in the bed.

(4) Radiation and the chemical reaction heat are the key factors affecting the bed temperature and the reduction time. The higher the magnesium content in the pellets is, the longer the reduction time is required due to the chemical reaction decalescence.

CRediT authorship contribution statement

Da-xue FU: Writing, Investigation, Analysis and interpretation of data; **Yao-wu WANG:** Investigation, Methodology; **Yue-zhong DI:** Visualization, Methodology; **Jian-ping PENG:** Visualization, Supervision; **Nai-xiang FENG:** Conceptualization, Supervision.

Declaration of competing interest

The authors declare that they have no known competing financial interests or personal relationships that could have appeared to influence the work reported in this paper.

Acknowledgments

This work was supported by the National Key Research and Development Program of China (No. 2021YFC29003205), the National Natural Science Foundation of China (Nos. 21878045, 51504058), the Fundamental Research Funds for the Central Universities, China (No. N2225019), and Natural Science Foundation of Liaoning Province, China (No. 2022-MS-106).

References

[1] CHE Yu-si, MAI Geng-peng, LI Shao-long, HE Ji-lin, SONG Jian-xun, YI Jian-hong. Kinetic mechanism of magnesium production by silicothermic reduction of CaO·MgO in vacuum [J]. Transactions of Nonferrous Metals Society of China, 2020, 30(10): 2812−2822. doi: 10.1016/S1003-6326(20)65423-1

[2] CHU Cheng-lin, HAN Xiao, BAI Jing, XUE Feng, CHU Paul-kao. Surface modification of biomedical magnesium alloy wires by micro-arc oxidation [J]. Transactions of Nonferrous Metals Society of China, 2014, 24(4): 1058−1064. doi: 10.1016/S1003-6326(14)63162-9

[3] XIONG Neng, TIAN Yang, YANG Bin, XU Bao-qiang, DAI Tian, DAI Yong-nian. Results of recent investigations of magnesia carbothermal reduction in vacuum [J]. Vacuum, 2019, 160: 213−225. doi: 10.1016/j.vacuum.2018.11.007

[4] FU Da-xue, WANG Yao-wu, ZHANG Ting'an, FENG Nai-xiang. Review on the silicothermic process for primary magnesium production [J]. Metallurgical and Materials Transactions B, 2023, 54B: 1−21. doi:10.1007/s11663-022-02695-z

[5] TIAN Yang, WANG Li-peng, YANG Bin, DAI Yong-nian, XU Bao-qiang, WANG Fei, XIONG Neng. Comparative evaluation of energy and resource consumption for vacuum carbothermal reduction and Pidgeon process used in magnesium production [J]. Journal of Magnesium and Alloys, 2020, 10(3): 697−706. doi: 10.1016/J.JMA.2020.09.024

[6] HUA Jin, HE Li-le, YAN Ke-ding, WANG Min. Robotic slag offloading and process improvement of magnesium smelting in Pidgeon process with faster region-based convolutional neural network [J]. International Journal of Heat and Technology, 2019, 37(1): 345−350. doi: 10.18280/ijht.

370141

[7] HUA Jian-she, XUE Chen, LI Fang. Application research of artificial neural network in magnesium reduction rate prediction [J]. Light Metal (China), 2013(12): 43−46. (in Chinese) doi: 10.13662/j.cnki.qjs.2013.12.013

[8] HU Wen-jiang, JIANG Jie, AN Shi-qi. A Continuous burden control system for magnesium production [J]. Nonferrous Metals Engineering (China), 2005, 57(2): 98−100. (in Chinese) doi: 10.3969/j.issn.2095-1744.2005.02.026

[9] FENG Nan, AO Wen-qing. Development and application of regenerative pulse combustion control technology [J]. Industrial Furnace (China), 2013, 35(6): 12−15. (in Chinese) doi: 10.3969/j.issn.1001-6988.2013.06.004

[10] REN Ling, XIA De-hong, REN Chun-xiao. Numerical simulation and application of large magnesium reduction furnace based on regenerative combustion technology [J]. Nonferrous Metals, 2012(3): 26−30. (in Chinese) doi: 10.3969/j.issn.1007-7545.2012.03. 008

[11] LIANG Wen-yu, SUN Xiao-lin, LI Feng-shan, LI Min, DAI Wen-bin. Research progress on magnesium smelting methods [J]. China Nonferrous Metallurgy, 2020, 49(4): 36−44, 53. (in Chinese) doi:10.19612/j.cnki.cn11-5066/tf. 2020.04.009

[12] YOU Jing, WANG Yao-wu. Reduction mechanism of Pidgeon process of magnesium metal [J]. The Chinese Journal of Process Engineering, 2019, 19(3): 560−566. (in Chinese) doi: 10.12034/j.issn.1009-606X.218236

[13] MAJID S, SINA N O, ALIREZA S, MOHAMMAD H S. Improving service life of magnesium reduction steel retorts against creep collapse by structural modification [J]. Engineering Failure Analysis, 2020, 113: 104551. doi:10.1016/j. engfailanal.2020.104551

[14] MU Xiao-hui, LUO Hong-jie, WANG Yao-wu, FENG Nai-xiang. Research progress on agent in thermal magnesium reduction process [J]. Light Metals (China), 2014(2): 45−49. (in Chinese) doi: 10.13662/j.cnki.qjs.2014. 02.012.

[15] FU Da-xue, WANG Yao-wu, PENG Jian-ping, DI Yue-zhong, TAO Shao-hu, FENG Nai-xiang. Comparison of extracting magnesium by aluminothermic reduction and Pidgeon process [J]. Advanced Materials Research, 2012, 550: 1779−1783. doi:10.4028/www.scientific.net/AMR.550-553. 1779

[16] FU Da-xue, WANG Yao-wu, PENG Jian-ping, DI Yue-zhong, TAO Shao-hu, FENG Nai-xiang. Kinetics and mechanism of vacuum isothermal reduction of magnesia by aluminum [J]. Canadian Metallurgical Quarterly, 2016, 55(3): 365−375. doi: 10.1080/00084433.2016.1195053

[17] WANG Yao-wu, YOU Jing, PENG Jian-ping, DI Yue-zhong. Production of magnesium by vacuum aluminothermic reduction with magnesium aluminate spinel as a by-product [J]. JOM, 2016, 68(6): 1728−1736. doi: 10.1007/s11837-016-1865-6

[18] ZHANG Teng, DU Shuang-ming, SUN Wan-cheng, ZHANG Ju-mei, NIU Li-bin, ZHENG Bin, HUA Xiao-hu. Novel method to prepare magnesium by aluminothermic reduction of magnesia and calcium hydroxide at normal atmosphere, 1223 K (950 °C) [J]. Metallurgical and Materials Transactions B, 2017, 48B: 488−496. doi: 10.1007/s11663-016-0821-8

[19] LIU Zhan-qi, LIU Jia-xiang, JIANG Bing, QIU Qian. Process for preparing magnesium from dolomite by vacuum aluminothermic reduction [J]. Nonferrous Metals, 2010, 62(2): 56−58. (in Chinese) doi: 10.3969/j.issn.2095-1744. 2010.02.014

[20] WANG Yao-wu, PENG Jian-ping, DI Yue-zhong, FENG Nai-xiang, LI Meng. Extraction of magnesium from calcined magnesite by aluminothermic reduction in vacuum [J]. Chinese Journal of Vacuum Science Technology, 2013, 33(7): 704−708. (in Chinese) doi: 10.3969/j.issn.1672-7126.2013. 07.16

[21] YANG Jian, KUWABARA M, SAWADA T, SANO M. Kinetics of isothermal reduction of MgO with Al [J]. ISIJ International, 2006, 46(8): 1130−1136. doi:10.2355/ isijinternational.46.1130

[22] FU Da-xue, WANG Yao-wu, PENG Jian-ping, DI Yue-zhong, TAO Shao-hu, FENG Nai-xiang. Mechanism of extracting magenesium from mixture of calcined magnesite and calcined dolomite by vacuum aluminothermic reduction [J]. Transactions of Nonferrous Metals Society of China, 2014, 24(8): 2677−2686. doi: 10.1016/S1003-6326(14)63398-7

[23] YANG Jian, KUWABARA M, LIU Zhong-zhu, ASANO T, SANO M. In situ observation of aluminothermic reduction of MgO with high temperature optical microscope [J]. ISIJ International, 2006, 46(2): 202−209. doi:10.2355/ isijinternational.46.202

[24] XU Xiang-bin, Cao Hui-jun. Review of the performance of different reducer during the thermal reduction of magnesium [J]. Light Metals (China), 2016(4): 49−51. (in Chinese) doi: 10.13662 /j.cnki.qjs.2016.04.012

[25] FENG Nai-xiang, WANG Yao-wu. A method of producing magnesium by vacuum thermal reduction using magnesite and dolomite as materials [J]. The Chinese Journal of Nonferrous Metals, 2011, 21(10): 2678−2686. (in Chinese) doi: 10.19476/j.ysxb.1004.0609.2011.10.033

[26] DI Yue-zhong, WANG Zhi-hui, WANG Yao-wu, PENG Jian-ping, FENG Nai-xiang. Extract of high-whiteness aluminum hydroxide from residues of novel process of magnesium production by aluminothermic reduction [J]. CIESC Journal, 2013, 64(3): 1106−1111. (in Chinese) doi: 10.3969/j.issn.0438-1157.2013.03.045

[27] SHU Hui, WU Lin-li, LUO Hong-jie, ZHANG Min, LIU Jun. Production of Mg−Ca alloy by one-step vacuum aluminothermic reduction [J]. Chinese Journal Vacuum Science and Technology, 2019, 39(5): 434−440. (in Chinese) doi: 10.13922/j.cnki.cjovst.2019.05.13

[28] YANG Zhan-tao, DUAN Dong-ping, YOU Zhi-gang. Preparation of Mg−Sr intermediate alloy by vacuum aluminothermic reduction [J]. Vacuum (China), 2015, 52(3): 42−45. (in Chinese) doi: 10.13385/j.cnki.vacuum. 2015.03.10

[29] HE Xiao-jun. Study on preparation of Mg−Li alloy by vacuum aluminothermic reduction [D]. Shenyang: Northeastern University, 2019. (in Chinese)

[30] FU Da-xue, FENG Nai-xiang, WANG Yao-wu, PENG Jian-ping, DI Yue-zhong. Kinetics of extracting magnesium from mixture of calcined magnesite and calcined dolomite by vacuum aluminothermic reduction [J]. Transactions of

Nonferrous Metals Society of China, 2014, 24(3): 839−847. doi: 10.1016/S1003-6326(14)63133-2

[31] FU Da-xue, WANG Yao-wu, PENG Jian-ping, DI Yue-zhong, FENG Nai-xiang. Improvements of Mg-extraction from magnesite and dolomite by aluminothermic reduction in vacuum [J]. Chinese Journal of Vacuum Science and Technology, 2014, 34(1): 60−67. (in Chinese) doi: 10.3969/j.issn.1672-7126.2014.01.13

[32] LI Rong-bin, ZHANG Chao, ZHANG Shao-jun, GUO Lie-jin. Experimental and numerical modeling studies on production of mg by vacuum silicothermic reduction of CaO·MgO [J]. Metallurgical and Materials Transactions B, 2014, 45B: 236−250. doi: 10.1007/s11663-013-9934-5

[33] ZHANG Chao, CHU Hua-qiang, GU Ming-yan, ZHENG Shu. Experimental and numerical investigation of silicothermic reduction process with detailed chemical kinetics and thermal radiation [J]. Applied Thermal Engineering, 2018, 135: 454−462. doi: 10.1016/j.applthermaleng.2018.02.091

[34] LI R B, ZHANG S J, GUO L J, WEI J J. Numerical study of magnesium (Mg) production by the Pidgeon process: Impact of heat transfer on Mg reduction process [J]. International Journal of Heat and Mass Transfer, 2013, 59: 328−337. doi: 10.1016/j.ijheatmasstransfer.2012.09.027

[35] XU Ri-yao. Magnesium production by the silicothermic process [M]. Changsha: Central South University Press, 2003. (in Chinese)

[36] LIANG Lei, QIANG Jun-feng, WANG Xiao-gang, YANG Jian-sheng, TIAN Xin-wei, DENG Jun-ping, REN Jian-xun, FAN Zi-min, YU Zhu-huan. Study on deoxidizing pot interior temperature field by the silicothermic method refining magnesium technique [J]. Light metals (China), 2006(10): 58−61. (in Chinese) doi: 10.13662/j.cnki.qjs.2006.10.015

影响工业还原罐内铝热法炼镁过程还原效率的因素

傅大学[1,2]，王耀武[1,2]，狄跃忠[1,2]，彭建平[1,2]，冯乃祥[1,2]

1. 东北大学 多金属共生矿生态化冶金教育部重点实验室，沈阳 110819；
2. 东北大学 冶金学院，沈阳 110819

摘　要：在工业还原罐内进行铝热还原炼镁试验，分析影响还原效率的因素。结果表明：结晶镁的氧化和燃烧以及原料混合不均匀是导致还原效率降低的主要原因；原料混合不均匀导致贫铝区和 MgO 剩余，促进生成 $12CaO·7Al_2O_3$ 和 $CaO·Al_2O_3$；对于富铝区域，MgO 和 CaO 同时被还原，生成 Mg_2Ca 相。辐射传热和化学反应吸热是影响还原速率的关键因素；提高加热温度能够迅速提高球团层的温度，进而使球团获得足够的反应速度；此外，球团中含镁量越高，需要的反应时间越长。

关键词：镁冶金；真空铝热还原；皮江法；传热

(Edited by Bing YANG)